JOURNAL OF CATALYSIS 119, 483–496 (1989)

Mixed Reactant Photocatalysis: Intermediates and Mutual Rate Inhibition

CRAIG S. TURCHI AND DAVID F. OLLIS

Department of Chemical Engineering, North Carolina State University, Raleigh, North Carolina 27695-7905

Received March 7, 1989; revised June 12, 1989

Near UV-illuminated slurries of titanium dioxide were used to study the photocatalyzed degradation kinetics of benzene and perchloroethylene (PCE) as water contaminants. In all runs, the concentration(s) of reactant(s) (initially 15–500 μM) as well as the evolution of CO_2 final product were monitored. The single component initial rate data were well described by Langmuir–Hinshelwood rate forms, and integration of these rate equations provided simulations of the entire time course of each reaction. Perchloroethylene degraded completely without any evidence of kinetically significant chemical intermediates; however, adequate simulation of the benzene time course data required the incorporation in the model of at least two reaction intermediates. Subsequent GC/MS analysis of a benzene reaction slurry revealed several intermediate species, with positive identification of phenol and quinone. Using the kinetic rate parameters obtained from the single component initial rate data and including competitive intermediate terms, the Langmuir–Hinshelwood rate form was able to simulate the results of several binary reactant experiments. The data showed that the effect of PCE concentration on benzene reaction rate was negligible, while benzene and its intermediates significantly inhibited PCE degradation. Simulations with this simple model for diminution of both reactants as well as CO_2 product evolution were quite good for low initial reactant concentrations, but overestimated the competitive inhibitory effect of high ($\approx$ 300 μM) initial PCE concentrations.

INTRODUCTION

Photoassisted heterogeneous catalysis has been gaining attention as a technique for total destruction of hydrocarbon and chlorocarbon contaminants in water. The catalyzed process is achieved by the illumination of a semiconductor catalyst, typically titanium dioxide, with greater-than-bandgap ultraviolet or near ultraviolet light in order to create electron excitation within the solid. The photoexcitation event forms electron–hole pairs, some of which migrate to the semiconductor surface. Interaction of these conduction-band electrons and valence-band holes with adsorbates, thought to be oxygen and water or hydroxyl groups, respectively, leads to the formation of hydroxyl and other oxygen-containing radicals (*1–5*). These radicals may then attack and oxidize organics in the system. In general, oxidation of low concentration hydrocarbon and chlorocarbon solutes in water has been reported to be complete, with the final products being innocuous CO_2 and HCl.

While many typical water pollutants and related compounds have been successfully mineralized via photocatalysis (*6–8*), the establishment of kinetic models with a wide range of validity has been somewhat slow. Studies have shown that a Langmuir–Hinshelwood rate form can adequately describe the *initial* rate of single reactant disappearance of most systems (*6, 7*), yet the use of rate modeling to predict concentration versus time (hereafter denoted as temporal) data has not been documented. Additionally, almost no studies have investigated systems of more than one reactant (*9, 10*). The added complexity of multicomponent systems, with several reactants and numerous possible intermediates, has previously hampered efforts to model such systems. Kinetic models which describe the time course of reaction are necessary to

0021-9517/89 $3.00

foster growth of photocatalytic reactor and process design, especially since the potential utility of photocatalysis for water purification rests on the ability of the catalyst to carry out very high conversion of oxidizable water contaminants.

In this study, we determine the initial degradation rate and temporal behavior of a well-defined binary reactant system: perchloroethylene (PCE) and benzene. This pair was chosen because (i) PCE degradation is reported to be both rapid and kinetically "clean"; that is, it proceeds without generation of measurable intermediates (*11, 12*); (ii) benzene is expected to proceed to mineralization via one or more important intermediates (as 6 CO_2 molecules clearly cannot be produced in a few simple steps); (iii) both reactants have been previously degraded photocatalytically in this and other laboratories (*11, 13*); and (iv) these reactants and their potential intermediates are not likely to interfere with each other during gas chromatographic analysis. The versatility of the Langmuir–Hinshelwood rate form is tested by obtaining rate parameters from initial rate data for single component degradations, and then examining its application for prediction of temporal and multicomponent behavior. The kinetic influence of degradation intermediates is also investigated and incorporated into the kinetic model.

EXPERIMENTAL

The catalyst used in these experiments was P25 TiO_2 supplied by the Degussa Corp. On the basis of the manufacturer's information, the primary particle diameter was 30 nm with a surface area of 50 ± 15 m^2/g. The crystal structure was primarily anatase. The P25 particles were spherical and nonporous, with a composition of >99.5% TiO_2. Impurities included: Al_2O_3 (<0.3%), HCl(<0.3%), SiO_2(<0.2%), and Fe_2O_3(<0.01%). While these levels were low in terms of bulk composition, it was possible that impurities (particularly iron) segregated at the photocatalyst surface and may have had a significant effect on electron transfer to and from adsorbates. The powdered semiconductor catalyst was used as supplied, without any pretreatment. The benzene was spectrophotometric grade (99+% pure) purchased from Aldrich Chemical, while the perchloroethylene (PCE) was of similar grade, obtained from Eastman Kodak. The PCE contained 0.5% ethanol as an inhibitor.

Photocatalytic Reactor

A recirculating batch reactor similar to that used previously by Pruden and Ollis (*14*) was employed for these photocatalytic studies (Fig. 1). Catalyst loading in all kinetic runs was 0.001 weight fraction (1 g/liter), high enough to make the reactor slurry opaque to near UV radiation and found to give the most rapid degradation rate. The catalyst slurry was recirculated through a 300-ml quartz annular reactor. The reactor inner wall radius was 1.7 cm and the annular region itself was 0.6 cm thick. Seven 15-W blacklight-blue fluorescent bulbs (Sylvania F18T8/BLB) provided illumination, with one lamp mounted down the center of the reactor and the others surrounding the outside. Since the lamps emitted radiation almost exclusively in the region of 310–500 nm, direct photon absorption by these organic reactants was expected to be minimal. A recirculation reservoir provided inlet ports for a dissolved carbon dioxide probe and a thermometer. In the binary reactant experiments, the total circulating liquid volume was 700 ml, leaving a 210-ml gas headspace in the reservoir to supply sufficient oxygen for the oxidation. A 600-ml liquid volume was used for the single component runs. Prior to most runs, the TiO_2 slurry was illuminated and O_2 sparged for 1 h to break down any possible organic water impurities remaining in the system and to remove any CO_2 present. Sparging the circulating reactor slurry with pure O_2 also served to equilibrate the dissolved oxygen level and to fill the headspace with oxygen before the PCE

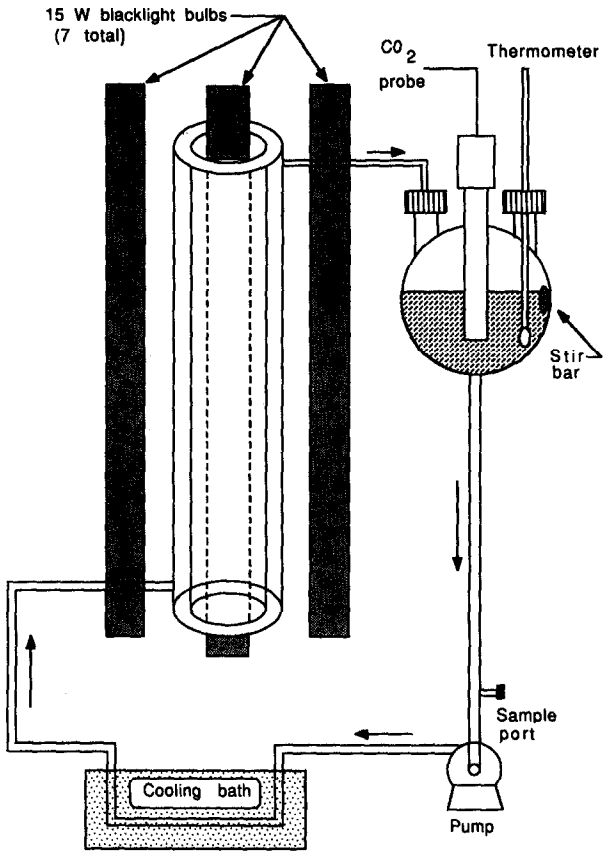

Fig. 1. Photocatalytic reactor.

and/or benzene reactants were loaded and the system sealed. This procedure provided sufficient excess oxygen so that, for the highest reactant loadings, only 15–20% of the total available oxygen was consumed. To enhance the mass transfer of oxygen from the headspace to the liquid, a magnetic stir bar was mounted vertically to agitate the gas–liquid interface. A magnetic drive pump circulated the slurry through a cooling coil to maintain the solution temperature at 20 ± 1°C before returning it to the reactor. All tubing was constructed of glass; thus only glass, Teflon, and the polypropylene pump head contacted the slurry solution.

Analyses

Reactant concentrations were monitored with a Perkin–Elmer Sigma 1 gas chromatograph. Liquid reactor samples were placed in vials, sealed with Teflon-faced septa, and allowed to equilibrate at 30°C. Vapor samples from the vial headspace were then injected into the GC. The use of isothermal conditions with a 1% AT-1000 packed column (Alltech Associates) allowed for detection of liquid phase reactant concentrations as low as 0.1 μM. For analysis of intermediates (which were expected to be nonvolatile), samples from the reactor slurry were acidified to pH < 2 and extracted with methylene chloride. Molecules containing carbon ring structures, that is, those likely to be benzene degradation intermediates, strongly favor an organic phase at this pH even if they are highly hydroxylated (*15*). Therefore, this extraction was expected to isolate any nonvolatile ring compounds present in the slurry.

The extract was concentrated by evaporation of the CH_2Cl_2 solvent and injected into a Perkin–Elmer GC/mass spectrometer.

Evolved CO_2 was measured in the reactor by a HNU gas-sensing electrode. Use of the CO_2 probe required that the system pH be kept constant; hence a phosphate buffer (0.1 *M* NaH_2PO_4) was used to keep the slurry at pH 4.5. At this pH, all dissolved carbonate species were in the nonionized forms of CO_2 and H_2CO_3 (pK_{a1} = 6.38 at 20°C), allowing both for their detection in the liquid phase by the probe and for the use of a Henry's Law coefficient, H_i, to determine the gas phase CO_2 concentration (*16*, *17*). The assumption of equilibrium between the gas and liquid phases in the reactor reservoir was necessary for calculation of the amount of CO_2 and organic reactant in the headspace by Henry's Law. For the binary reactant experiments, 6% of the total benzene and 17% of the total PCE were in the headspace at any given time.

Photon flux into the reactor was determined by potassium ferrioxalate actinometry following the technique of Hatchard and Parker outlined by Rabek (*18*). The modifications of Dennis and Roth (*19*) were followed as these were found to yield better reproducibility. For the seven-lamp system used, a rate of 1.1×10^{-3} einstein(mol photon)/min entered the reactor, based on reaction with the TiO_2-free actinometry solution. This figure represented the maximum possible photon absorption rate for the photocatalyst during degradation runs. The actual absorption by TiO_2 slurries would be less due to (i) the scattering of some light out of the reactor when the TiO_2 particles were present and (ii) the fact that the ferrioxalate actinometer solution absorbed all entering photons, while only those of wavelength less than 380 nm possessed sufficient energy to excite the photocatalyst. These actinometry experiments were run under darkroom conditions in order to eliminate interference from ambient light. The precaution of darkroom conditions was not necessary during the degradation runs since the ambient room light was not energetic enough to excite the photocatalyst. This fact was established by a blank (UV light off) run.

The sequence of experimental runs began with the photocatalyzed degradation of single component systems. Benzene was degraded under both air-equilibrated and oxygen-equilibrated conditions for a variety of initial concentrations. Runs were then completed with PCE as the only reactant. From these single component runs, kinetic rate parameters were determined. Because we monitored both original reactant and CO_2 final product concentration simultaneously, we were able to deduce clearly both the need for and the likely minimum number of kinetically important intermediates in the multistep degradation of benzene. Finally, a series of binary experiments was carried out; the initial conditions for these runs are listed in Table 1.

RESULTS

Before the kinetic experiments were begun, the optimum catalyst loading for this reactor geometry was determined. Figure 2 displays the variation of initial rate of degradation vs photocatalyst loading for experiments with an initial PCE concentration of

TABLE 1

Initial Concentrations in the Binary Experiments

Run	C_B^0 (μM)	C_P^0 (μM)
B0	147	100
B1	393	313
B2	394	110
B3	400	27.2
B4	121	282
B5	126	105
B6	124	24.0
B7	32.6	302
B8	32.6	101
B9	32.5	24.6
B10	367	168

Note: Total μmoles of each reactant initially in the system is given by $(V_L + H_i V_G)C_i^0$.

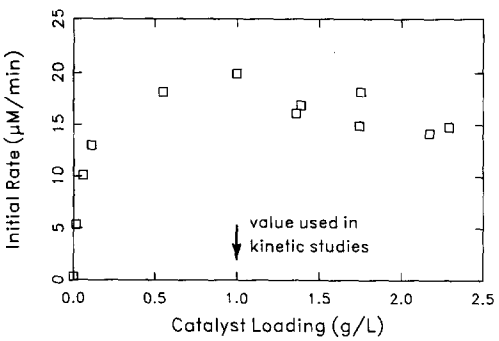

Fig. 2. Variation of initial reaction rate with TiO_2 photocatalyst concentration. Initial concentration in each run = 209 μM PCE.

209 μmol/liter. The plot shows a broad maximum in initial reaction rate around 0.001 weight fraction TiO_2. Investigation of the absorbance by TiO_2 slurries of 350-nm photons (the primary emitted wavelength of our lamps) has shown that, at this catalyst concentration, the thin annular region of the reactor is opaque. The gradual decrease in reaction rate at higher loadings is thought to be related to increased scattering of photons out of the reactor as catalyst concentration near the inner reactor wall is increased (*20*).

To verify that reactant disappearance was due entirely to the photocatalytic mechanism, a run was carried out without illumination. After 360 min (6 h), virtually no decrease in benzene concentration was seen, while the PCE concentration dropped by roughly 20%. The decrease in PCE concentration was believed to be due to its tendency to leak very slowly through the seals of the reservoir and through the punctured Teflon septum of the sample port (*21*). In the presence of illuminated photocatalyst, the PCE concentration usually decreased to below detectable levels (<0.1 μM) within 60 min; hence the slow leakage rate was not detrimental to the kinetic study. Obviously, degradation experiments involving volatile organics must be carried out in a tightly closed system. Finally, since neither benzene nor PCE directly absorbed light of wavelength >300 nm, homogeneous photoreaction did not play a role in the degradation of the primary reactants. In contrast, intermediate species may undergo homogeneous photolysis if they are capable of absorbing near UV photons (e.g., quinones) (*11*).

Headspace–Liquid Mass Transfer Considerations

The assumption of gas–liquid equilibrium within the reactor reservoir was tested in two fashions. In one experiment, liquid-phase CO_2 was monitored by the HNU probe while headspace CO_2 was followed by recirculation of the headspace through a Horiba PIR 2000 infrared carbon dioxide analyzer. When illumination was initiated, the CO_2 responses from both monitors rose in parallel and followed similar courses, reaching plateaus at the same time. This parallel response showed that the CO_2 formed by the degradation reaction in the liquid phase was rapidly equilibrated with the gas headspace, implying an insignificant gas–liquid mass transfer resistance.

A subsequent set of experiments provided a determination of the mass transfer conductance between the gas headspace and the liquid phase. The resulting value of k_La = 0.13 liter/min corresponded to a maximum mass transfer rate of twice the maximum observed (binary) reaction rate. Evidence that the photodegradations in this study were not oxygen-influenced resulted from the equivalent initial disappearance rates found for benzene under air- or oxygen-saturated conditions (Fig. 3). Other researchers have found that, under oxygen limitation, the reaction rate dependence on O_2 follows a Langmuir–Hinshelwood form (*1, 4, 22*),

$$r^0 \propto \frac{K_{O_2}C_{O_2}}{1 + K_{O_2}C_{O_2}}. \qquad (1)$$

For the Degussa P25 TiO_2 of our study, Sczechowski found K_{O_2} = 110 atm^{-1} (*22*). For this value, catalyst oxygen sites in the air-equilibrated system were 96% saturated

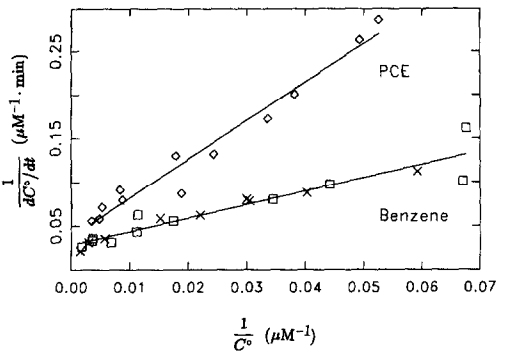

Fig. 3. Results of single component *initial rate* studies. (×) Benzene, air-equilibrated; (□) benzene, oxygen-equilibrated; (◇) PCE, oxygen-equilibrated. Lines are least-squares fits from which kinetic parameters (Table 2) for Eq. (4) were determined.

with O_2 and no noticeable increase in rate should be expected for the pure O_2-equilibrated system, in agreement with the observed results. All experiments, except the previously mentioned benzene reactant runs, were run with an oxygen saturated system so that the sealed reactor would contain a sufficient excess of O_2.

Total Carbon Mass Balance

Closure of the carbon mass balance was achieved by comparing the carbon evolved as CO_2 with the initial loading of organic reactants. Early calibrations showed that although the CO_2 probe gave a good, highly linear voltage response vs log C_{CO_2}, slight fluctuations in the intercept of the calibration line caused, because of the Nernstian logarithmic voltage vs concentration relation, relatively large (sometimes ±30%) variations in the calculated total CO_2. Use of the gas-phase infrared CO_2 analyzer for some experiments demonstrated closure of the carbon balance for each run. Thus, while the slope of the CO_2 electrode calibration line was a reliable measure of the proportionality between the logarithm of CO_2 concentration and the voltage output, the intercept of the calibration line was too sensitive to slight variations. Subsequently, the intercept of the CO_2 probe calibration line was adjusted slightly to bring about closure of the carbon mass balance. This adjustment never exceeded 6% of the intercept value obtained from a linear least-squares best fit of the calibration line.

The Langmuir–Hinshelwood (L–H) rate form for conversion of total reactant mass i_{total} as a function of limiting reactant i is

$$-\frac{di_{total}}{dt} = \frac{k_i K_i C_i}{1 + K_i C_i} V_L, \qquad (2)$$

where the *illumination time* was used for all rate determinations. This measure refers to how long each circulating solution element was in the illuminated zone of the reactor, that is, three sevenths of the actual run time for the binary experiments. Since the total amount of reactant in the system (liquid and headspace) was given by $i_{total} = (V_L + H_i V_G)C_i$,

$$-(V_L + H_i V_G)\frac{dC_i}{dt} = \frac{k_i K_i C_i}{1 + K_i C_i} V_L. \qquad (3)$$

Defining $\beta = (V_L + H_i V_G)/V_L$ and inverting Eq. (3) yields

$$-\frac{1}{dC_i/dt} = \left(\frac{\beta}{k_i K_i}\right)\frac{1}{C_i} + \frac{\beta}{k_i}. \qquad (4)$$

The linear appearance of plots of reciprocal initial rate vs reciprocal initial concentration (Fig. 3) verified the applicability of the L–H rate form (Eq. (3)) to all single component solutions. The slopes and intercepts of the lines in Fig. 3 provided the reactant initial rate kinetic parameters, k_i and K_i, for the model (Table 2). The initial disappearance rate was based on the decrease in the total amount of reactant in the reactor, including the headspace region. Carbon dioxide evolution was followed in all single and binary component runs. For the PCE experiments, stoichiometric CO_2 formation was almost instantaneous with the observed decrease in reactant concentration and the CO_2 curve reached a plateau as soon as the PCE concentration became undetectable (Fig. 4). With benzene, a significant lag time was observed between ben-

TABLE 2

Kinetic Parameters Used in Eqs. (3), (6)–(10)

Species	i	k_i (μM/min)	K_i (μM^{-1})
Benzene	B	39	0.018
Perchloroethylene	P	34	0.0086
Intermediate	I	8	0.015

Note: Benzene and PCE values from single component initial rate data of Fig. 3. Intermediate values determined from a best fit to benzene experimental data. Parameters were based on time spent in the illuminated zone of the reactor.

zene disappearance and the evolution of the corresponding stoichiometric amount of CO_2 (Fig. 5, data). Similar trends in the CO_2 data were noted in the binary (PCE and benzene) experiments depending on the relative concentrations of the reactants.

DISCUSSION

The L–H rate form (Eq. (3)) described the single component *initial rate* data very well for the concentration ranges examined (Fig. 3). The corresponding L–H parameter values (Table 2) for benzene and PCE were used in all subsequent model simulations unless otherwise stated.

From the traditional derivation of L–H kinetics, K represents the equilibrium adsorption (or binding) constant of the reactant while k is a measure of the intrinsic reactivity at the surface. The mechanism(s) of the photocatalytic degradation has not been unequivocally determined; thus the fundamental meaning of the model parameters is unclear. There is considerable evidence in the literature which implicates OH$^\cdot$ as the primary oxidizing species. This evidence includes: (i) ESR identification of OH$^\cdot$ in illuminated TiO_2 slurries (*5, 23–25*); (ii) the fact that aqueous TiO_2 is highly hydroxylated (*26–28*) and surface hydroxyls may readily undergo oxidation to hydroxyl radicals (*3, 23, 28, 29, 35, 36*); (iii) the formation of hydroxylated intermediates (*1, 4, 9, 11, 37*) similar to those formed by reactions known to involve OH$^\cdot$ (*38, 39*); (iv) little or no reaction in oxygenated, nonaqueous media (*2, 40, 41*); and (v) the observation of a kinetic isotope effect for the D_2O–H_2O substitution (*42*). Rate forms similar to Eq. (3) can be derived under a variety of assumptions concerning where the oxidation of the organic occurs, e.g., for cases of surface-generated OH$^\cdot$ attacking the organic at the photocatalyst surface or in the solution phase (*43*). These arguments do not lessen the empirical value of this rate form; however, care must be taken in assigning fundamental meaning to the values obtained. A subsequent paper will discuss rate forms and parameters derived from hydroxyl radical attack mechanisms (*43*).

The appropriate parameter values were used in the integrated form of Eq. (3) to

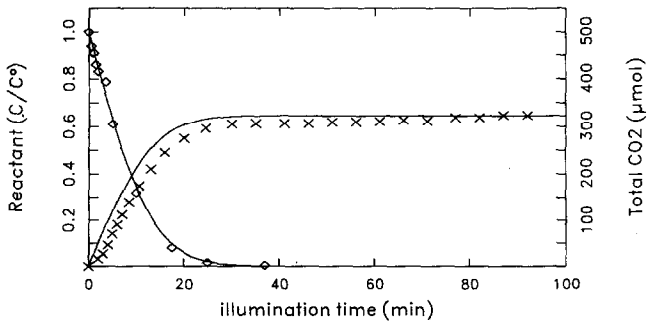

Fig. 4. Single component PCE run. (◇) PCE, (×) CO. Lines are the model prediction based on Eq. (3) and using the parameters from Table 2. Initial concentrations: $C_B^0 = 0\ \mu M$, $C_P^0 = 207\ \mu M$.

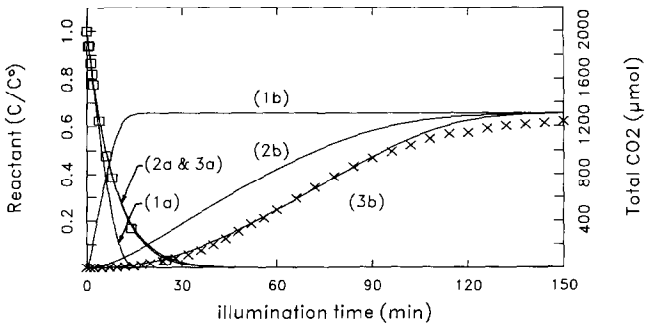

Fig. 5. Single component benzene run. (□) Benzene, (×) CO_2. Curves 1a and 1b are model predictions based on Eq. (3) where no intermediates are assumed. Curves 2a and 2b are a best fit assuming one intermediate. Curves 3a and 3b assume two intermediates (Eqs. (6)–(10), parameters from Table 2). Initial concentrations: $C_B^0 = 279\ \mu M$, $C_P^0 = 0\ \mu M$.

predict the temporal behavior of the reactant concentration in single reactant mineralization runs. Excellent agreement between the model prediction and the observed temporal data was found for the PCE experiments (Fig. 4) for all concentrations examined (19–282 μM). For the benzene reactant system, integration of Eq. (3) to give concentration predictions for the entire mineralization period resulted in considerable overestimation of the observed reaction rates for benzene disappearance and CO_2 appearance (Fig. 5, curves 1a and 1b). These deviations were most acute for the runs involving high initial benzene concentrations.

The observed benzene kinetics, coupled with the sigmoidal shape of the CO_2 product evolution data, were indicative of the production of kinetically important intermediate species during the reaction. These intermediates must have been long-lived enough to compete effectively with benzene for the reactive hydroxyl radicals (and related active oxygen forms) which drive the degradation. In the photocatalyzed degradation of chlorobenzene, a sequence of oxygenated intermediates including isomeric chlorophenols and benzoquinones, as well as hydroquinone and catechol, have been identified as long-lived intermediate species (*11*). Similar hydroxylated aromatic intermediates have been witnessed in the photocatalyzed degradation of phenol (Fig. 6) (*1, 4*), 4-chlorophenol (*9*), and 2,4,5-trichlorophenoxyacetic acid (*37*). Thus, during the process of attack on the aromatic reactant, hydroxylations, ring opening, carboxylate formation, and eventual decarboxylations were likely to take a substantial period of time, with each successive molecular intermediate produced also competing for the attacking radicals. In the case of PCE, no such lengthy process is probable since possible PCE intermediates such as dichloroacetyl chloride ($Cl_2C{=}C(OH)Cl$), dichloroacetaldehyde (Cl_2HCCHO), or phosgene are known to rapidly degrade under the existing conditions (*12*). Previous experimenters had detected no intermediates during PCE destruction (*12*) and no evidence of PCE-derived intermediates was found in the present study.

To account for probable benzene-derived intermediates, a term for a competitively adsorbing intermediate was added to Eq. (3). Inclusion of one intermediate brought the predictions of benzene disappearance into agreement with the observed values but did not provide sufficient sigmoidal CO_2 evolution curves (Fig. 5, curves 2a and 2b). Thus it was assumed that more than

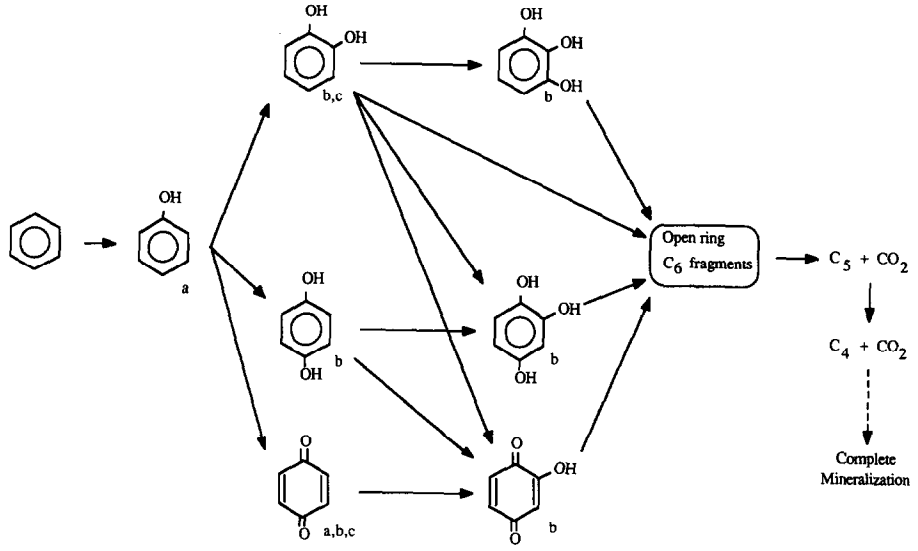

Fig. 6. Suggested photocatalytic degradation pathway for benzene. (a) Detected in this study, (b) detected by Okamoto *et al.* in the photocatalytic degradation of phenol (*4*), (c) detected by Augugliaro *et al.* in the photocatalytic degradation of phenol (*1*). Note that attack at the *ortho* or *para* position is favored.

one intermediate was involved and the following simple reaction path was suggested:

$$B \rightarrow I_1 \rightarrow I_2 \rightarrow 6CO_2. \qquad (5)$$

In view of the similar reactivity expected of oxygenates and to avoid needless complexity, the intermediate kinetic parameters were assumed to be equal: $k_{I_1} = k_{I_2} = k_I$ and $K_{I_1} = K_{I_2} = K_I$. The intermediate parameters were chosen to give the best fit to the benzene *single component* data. Incorporation of two intermediate terms allowed the model to simulate the single component benzene degradation and CO_2 evolution curves with reasonable accuracy (Fig. 5, curves 3a and 3b). It should be noted that introducing three, four, or more intermediate terms would provide equivalent or better fits of the data; however, a minimum of two were sufficient to represent the reactant and final product kinetics.

Detection of Intermediates

GC/MS analysis of the reactor solution from a benzene reactant experiment revealed the presence of several intermediate species. The oxygenated compounds phenol and quinone (1,4-benzoquinone) were detected as the major cyclic intermediate species present. Several other small peaks were detected by the GC/MS, including structures of molecular weights 124 and 216 g/mol, which were not unequivocally identified. Phenol and quinone were the only cyclic intermediates detected at appreciable concentrations, as the areas of other peaks seen were <10% of the quinone peak area. The conditions of the analysis did not allow for the detection of smaller ring fragment compounds. The species with molecular weight 124 may well have been 2-hydroxy-1,4-benzoquinone, identified by Okamoto *et al.* (*4*) as an intermediate in the photocatalyzed degradation of phenol (see Fig. 6). Two isomers of the compound with a molecular weight of 216 were detected. It seems likely that these species were a condensation product of two aromatic rings, similar to those reported by other researchers (*11, 29*).

The two major detected intermediates

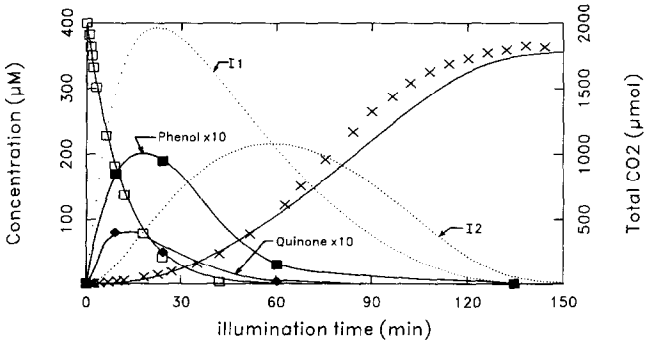

Fig. 7. Benzene single component run with detected cyclic intermediates. (□) Benzene, (×) CO_2, (■) phenol (×10), (◆) quinone (×10). Dotted curves are model predictions for intermediates based on the two-intermediate model (Eqs. (6)–(10)).

(phenol and quinone) were seen at concentrations much lower than the intermediate concentrations predicted (dotted lines, Fig. 7) by the two-intermediate model (Eqs. (6)–(10)). This was due to Eq. (5)'s oversimplification of the degradation mechanism. Since the observed amount of phenol and quinone could not account for the carbon mass-balance difference between benzene concentration and evolved CO_2, there must have been other intermediate species present in the reactor solution (e.g., Fig. 6). Another possibility was that significant quantities of intermediates, either phenol and quinone or other undetected ones, were tightly bound to the catalyst surface. (Based on 10^{15} sites/cm^2, there were 3.5×10^{20} catalyst surface sites in the reactor slurry. At a total concentration of 400 μM or less, binding of all organics would require less than one monolayer coverage.) Both conditions could account for the slow evolution of CO_2 and the low concentrations of phenol and quinone. The pathway of Eq. (5), though kinetically consistent, clearly oversimplifies the degradation mechanism.

Kinetic Model

To develop a kinetic rate model for the binary reactant system, the L–H form of Eq. (2), including intermediate terms, was extended to a two-component form:

$$-\frac{dB}{dt} = \frac{k_B K_B C_B}{1 + K_B C_B + K_P C_P + K_I(C_{I_1} + C_{I_2})} V_L \quad (6)$$

$$-\frac{dP}{dt} = \frac{k_P K_P C_P}{1 + K_B C_B + K_P C_P + K_I(C_{I_1} + C_{I_2})} V_L \quad (7)$$

$$\frac{dC_{I_1}}{dt} = \frac{k_B K_B C_B - k_I K_I C_{I_1}}{1 + K_B C_B + K_P C_P + K_I(C_{I_1} + C_{I_2})} \quad (8)$$

$$\frac{dC_{I_2}}{dt} = \frac{k_I K_I C_{I_1} - k_I K_I C_{I_2}}{1 + K_B C_B + K_P C_P + K_I(C_{I_1} + C_{I_2})} \quad (9)$$

$$CO_2 = 6(B^0 - B - C_{I_1} V_L - C_{I_2} V_L) + 2(P^0 - P). \quad (10)$$

Since the intermediates were expected to be hydroxylated aromatic compounds, they were assumed to be nonvolatile. Equations (6)–(10) were solved numerically using the k and K values given in Table 2 to obtain simulations of the binary experimental data. Figures 8–10 compare results for different initial reactant concentrations. For binary reactant runs with initial PCE concentrations of 25–100 μM and all examined

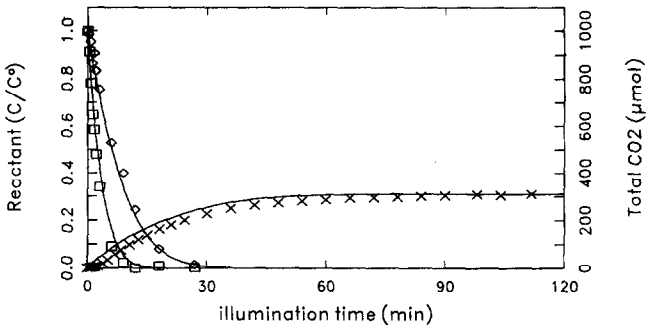

Fig. 8. Binary run B8. (□) Benzene, (◇) PCE, (×) CO_2. Curves are model predictions (Eqs. (6)–(10)) using the parameters of Table 2. Initial concentrations: $C_B^0 = 32.6\ \mu M$, $C_P^0 = 101\ \mu M$.

initial benzene concentrations (32–400 μM), the model tended to slightly overestimate the PCE reaction rate while giving excellent predictions of the benzene concentration and CO_2 evolution (e.g., Figs. 8 and 9). In the high ($C_P^0 \approx 300\ \mu M$) PCE runs, the predicted reaction rates were overly depressed. From the data it was apparent that the initial PCE concentration had little effect on the degradation rate of benzene. However, the K_P value obtained from the single component runs was fairly large; thus at higher PCE initial concentrations the model predicted a slower benzene reaction rate than was observed (Fig. 10). If it was assumed that benzene reaction was unaffected by PCE and the $K_P C_P$ term in the denominator of Eq. (6) was neglected, the predicted rate of benzene degradation agreed quite well with the data. Hence, it appeared that the benzene parameters described the binary system well, while those for PCE, specifically K_P, were too high. The binary data were fit better by lowering K_P substantially and raising k_P to keep the $k_P K_P$ product roughly equal. (The parameter values which gave the best fit to all the binary data were $k_P = 100\ \mu M$/min and $K_P = 0.002\ \mu M^{-1}$.) Such a modification produced excellent fits of the data within the framework of the L–H model but removed the utility of obtaining parameters for the binary model from the pure component data.

Several possibilities could explain the observed benzene inhibition of PCE degradation and simultaneous lack of effect of PCE on benzene reaction. First, there is a rea-

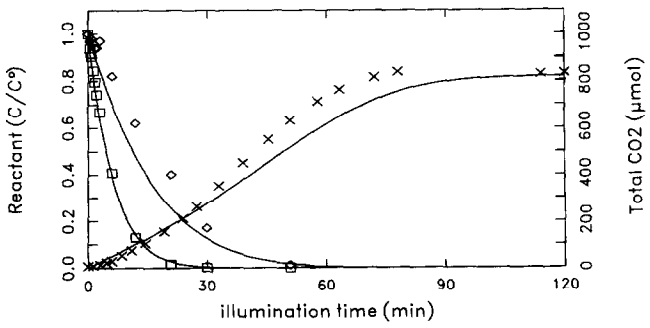

Fig. 9. Binary run B0. (□) Benzene, (◇) PCE, (×) CO_2. Curves are model predictions (Eqs. (6)–(10)) using the parameters of Table 2. Initial concentrations: $C_B^0 = 147\ \mu M$, $C_P^0 = 100\ \mu M$.

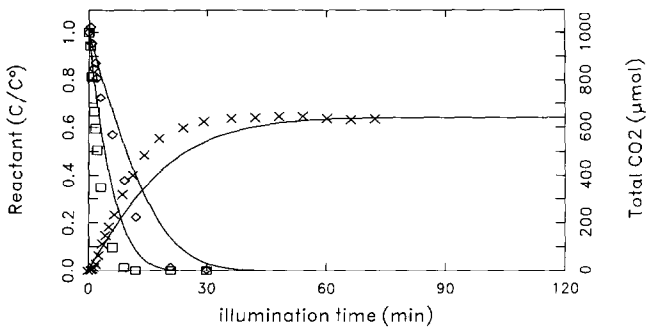

Fig. 10. Binary run B7. (□) Benzene, (◇) PCE, (×) CO_2. Curves are model predictions (Eqs. (6)–(10)) using the parameters of Table 2. Initial concentrations: $C_B^0 = 32.6\ \mu M$, $C_P^0 = 302\ \mu M$.

sonable amount of scatter in the PCE initial rate data (Fig. 3) which might allow slightly different estimates of k_P and K_P (i.e., from the calculated slope and intercept). However, this variation would be small and could not account for the entire discrepancy between the data and the model predictions. It seems likely that some mechanistic consideration, unaccounted for by the simple L–H model, is responsible for the specific inhibition of PCE. For instance, since TiO_2 is known to have different types of adsorption sites (*27, 30, 31*), benzene may be able to adsorb and react at all sites while PCE reaction is specific to one surface site. Thus the inhibitory effect of benzene on PCE would be more pronounced than that of PCE on benzene. Alternately, PCE may degrade primarily by reaction with solution phase radicals (through a mechanism to be explored in a subsequent paper (*43*)) while benzene adsorbs to (*32*) and reacts with hydroxyls on the catalyst surface. In this scenario, surface-bound benzene and its corresponding intermediates would intercept the majority of the surface-generated radicals before they could react with the solution-phase PCE. Lastly, some interaction between benzene and an excited PCE species may transfer energy to benzene, thus promoting benzene degradation and returning PCE to a nonreactive state. Clearly, additional mechanistic studies using radical and surface probing techniques are necessary before the true mechanism(s) responsible for the observed photocatalytic kinetic behavior can be determined.

Kinetic Simplifications

The ability to monitor both reactant and final product concentrations simultaneously demonstrated the kinetic influence of intermediates on total mineralization time and helped explain a curious result witnessed by several researchers investigating the photocatalytic degradation of aromatics. In a number of cases, L–H behavior has been reported for *initial* rate data but the full-time conversion has followed apparent first-order kinetics for much of each individual run (*1, 8, 33, 34*). If it is assumed that the degradation of aromatics is a step-wise process as in Eq. (5), and if the K values for these intermediates are fairly similar to the reactant K value, the denominator of the L–H equation may be simplified by the following approximation (*1, 33*).

$$1 + K_1C_1 + \sum_{i=2}^{n} K_iC_i \approx 1 + K_1C_1^0, \quad (11)$$

where C_1 represents the original reactant and $n - 1$ is the total number of kinetically important intermediates produced by the degradation. For experiments carried out in the same reactor, the K values of various

reactants are typically quite similar (*6, 7*), and for this particular study with benzene, the reactant and apparent intermediate K values were essentially identical (Table 2). The approximation of Eq. (11) produces a rate expression which yields L–H behavior for the initial rates (where $C = C^0$) while also describing the observed pseudo-first-order C vs t results. As displayed in Fig. 5, the success of this simplification results from the reactant concentration dropping to near zero while very little CO_2 product has yet evolved. During this early part of the total mineralization run, the primary reactant is replaced by intermediate species, thereby keeping the total oxidizable organic concentration relatively constant. The approximation not only simplifies the mathematical rate expression but also provides a more accurate estimation of overall conversion kinetics of the primary reactant based on initial rate derived parameters and without explicitly introducing intermediate terms into the model. However, as seen in Fig. 5, the decrease of original reactant concentration to zero does not correspond to the complete mineralization of all organics. Importantly, use of Eq. (11) for the PCE reactant system, where no important intermediates were present, resulted in notably poorer simulations of the observed data. Therefore, to use a modification such as Eq. (11), one must know whether intermediates significantly affect the degradation kinetics.

Finally, some photocatalysis studies have reported reactant equivalent "half-lives" rather than establishing a kinetic form (*8, 34*). At low reactant levels or for compounds which do not form important intermediates, the half-lives for reactant disappearance and for complete mineralization (CO_2 evolution) are similar, but at higher benzene (or similar reactant) levels where important intermediates occur, these two half-lives are quite different (e.g., Fig. 5). Since mineralization is the ultimate goal of water purification, this difference in half-lives illustrates the need for more complete temporal studies of contaminant mineralization.

CONCLUSIONS

Perchloroethylene and benzene were degraded to completion (mineralized) individually and in tandem in the presence of near UV-illuminated TiO_2. On the basis of the initial reactant loading, the stoichiometric amount of CO_2 was always eventually evolved. Initial rate data from single component runs provided kinetic parameters for use in a Langmuir–Hinshelwood rate expression. Integration of this expression gave predictions of the temporal reactant and CO_2 data. For PCE, these model simulations were in good agreement with the observed single component results and no evidence of kinetically important intermediates was found. In the benzene experiments, CO_2 evolution was preceded by the formation of relatively long-lived intermediate species. The single component benzene reactant model equations required addition of at least two intermediate terms in order to simulate accurately the observed CO_2 evolution.

In the binary reactant degradation experiments, PCE concentration had little effect on benzene reaction rate, while high benzene concentrations seriously retarded the PCE reaction. Extension of the pure component rate equation parameters to predict the binary degradation showed that the benzene parameters provided a good fit, but the PCE parameter values seriously overestimated the inhibitory effect of PCE at higher PCE concentrations. This observation implied that, while the $k_P K_P$ product was roughly correct, the value of K_P was too high. The results allow prediction of single component temporal data based on rate parameters from initial rate data and, while not entirely quantitative, are the most successful effort to date at predicting the complete temporal kinetics of a multicomponent system. Additionally, the importance of intermediates and their effect on the process time required to achieve total

mineralization were demonstrated. Finally, the use of CO_2 temporal data for quantitative mass balancing and for a diagnostic indication of the presence/absence of influential intermediates is clearly established in the present work.

More detailed kinetic and spectroscopic studies will be required in order to establish a clear mechanism for aromatic oxidation and mineralization and to unambiguously assign identities to important intermediates.

ACKNOWLEDGMENTS

We thank the National Science Foundation and Du Pont for fellowship support for C. S. Turchi during this study and Sandia National Laboratories for partial support during the preparation of this paper.

REFERENCES

1. Augugliaro, V., Palmisano, L., Sclafani, A., Minero, C., and Pelizzetti, E., *Toxicol. Environ. Chem.* **16,** 89 (1988).
2. Barbeni, M., Pramauro, E., Pelizzetti, E., Borgarello, E., Gratzel, M., and Serpone, N., *Nouv. J. Chim.* **8,** 547 (1984).
3. Matthews, R., *J. Chem. Soc. Faraday Trans. 1* **80,** 457 (1984).
4. Okamoto, K., Yamamoto, Y., Tanaka, H., Tanaka, M., and Itaya, A., *Bull. Chem. Soc. Japan* **58,** 2015 (1985).
5. Ceresa, E. M., Burlamacchi, L., and Visca, M., *J. Mater. Sci.* **18,** 289 (1983).
6. Ollis, D. F., *Environ. Sci. Technol.* **19,** 480 (1985).
7. Matthews, R., *J. Catal.* **111,** 264 (1988).
8. Pelizzetti, E., Barbeni, M., Pramauro, E., Serpone, N., Borgarello, E., Jamieson, M., and Hidaka, H., *Chim. Ind. (Milan)* **67,** 623 (1985).
9. Al-Ekabi, H., Serpone, N., Pelizzetti, E., Minero, C., Fox, M. A., and Draper, R. B., *Langmuir* **5,** 250 (1989).
10. DeBerry, D. W., Viehbeck, A., Peyton, G. R., and Karpinski, M., "Investigation of Photocatalytic Oxidation for Wastewater Cleanup and Reuse." US Dept. of Interior, No. RU-83/12, 1983.
11. Ollis, D. F., Hsiao, C., Budiman, L., and Lee, C., *J. Catal.* **88,** 89 (1984).
12. Hsiao, C., M.S. thesis, Univ. of California at Davis, 1983.
13. Matthews, R., *Wat. Res.* **20,** 569 (1986).
14. Pruden, L., and Ollis, D., *J. Catal.* **82,** 404 (1983).
15. Perry, R. H., and Chilton, C. H., Eds., "Chemical Engineer's Handbook," 5th Ed., p. **15**-6. McGraw-Hill, New York, 1973.
16. Butler, J. N., "Carbon Dioxide Equilibria and Their Applications. Addison-Wesley, Reading, MA, 1982.
17. Carbon Dioxide Electrode Manual ISE-10-22-00. HNU Systems, Inc., Newton, MA.
18. Rabek, J. F., "Experimental Methods in Photochemistry." Wiley, New York 1982.
19. Dennis, R. M., and Roth, J. A., "Potassium Ferrioxalate Actinometry and Homogeneous Photooxidation of Cyanide in a Laminar Flow Reactor," presented at New York A.I.Ch.E. Meeting, Nov. 1987.
20. Ayoub, P. M., and Dranoff, J. S., "A Model For Heterogeneous Photocatalytic Reactions In A Transport Reactor," presented at New York A.I.Ch.E Meeting, Nov. 1987.
21. Dietz, E. A., Jr., and Singley, K., *Anal. Chem.* **51,** 1809 (1979).
22. Sczechowski, J., M.S. thesis, North Carolina State Univ., 1988.
23. Jaeger, C. D., and Bard, A., *J. Phys. Chem.* **83,** 3146 (1979).
24. Anpo, M., Shima, T., and Kubokawa, Y., *Chem. Lett.,* 1799 (1985).
25. Howe, R. F., and Grätzel, M., *J. Phys. Chem.* **91,** 3906 (1987).
26. Doremieux-Morin, C., Enriquez, M. A., Sanz, J., and Fraissard, J., *J. Colloid Interface Sci.* **95,** 502 (1983).
27. Boehm, H. P., *Discuss. Faraday Soc.* **52,** 264 (1971).
28. Munuera, G, Rives-Arnau, V., and Saucedo, A., *J. Chem. Soc. Faraday Trans. 1* **75,** 736 (1979).
29. Fujihira, M., Satoh, Y., and Osa, T., *Bull. Chem. Soc. Japan* **55,** 666 (1982).
30. Tanaka, K., and White, J. M., *J. Phys. Chem.* **86,** 4708 (1982).
31. Yates, D. J. C., *J. Phys. Chem.* **65,** 746 (1961).
32. Nagao, M., and Suda, Y., *Langmuir* **3,** 786 (1987).
33. Okamoto, K., Yamamoto, Y., Tanaka, H., and Itaya, A., *Bull. Chem. Soc. Japan* **58,** 2023 (1985).
34. Al-Ekabi, H., and Serpone, N., *J. Phys. Chem.* **92,** 5726 (1988).
35. Clechet, P., Martelet, C., Martin, J. R., and Olier, R., *Electrochim. Acta* **24,** 457 (1979).
36. Sakata, T., Kawai, T., and Hashimoto, K., *J. Phys. Chem.* **88,** 2344 (1984).
37. Barbeni, M., Morello, M., Pramauro, E., Pelizzetti, E., Vincenti, M., Borgarello, E., and Serpone, N., *Chemosphere* **16,** 1165 (1987).
38. Barbeni, M., Minero, C., Pelizzetti, E., Borgarello, E., and Serpone, N., *Chemosphere* **16,** 2225 (1987).
39. Metelitsa, D. I., *Russ. Chem. Rev. (Eng. Transl.)* **40,** 7 (1971).
40. Fox, M.-A., and Chen, C., *J. Amer. Chem. Soc.* **103,** 6757 (1981).
41. Fujihira, M., Satoh, Y., and Osa, T., *J. Electroanal. Chem.* **126,** 277 (1981).
42. Cunningham, J., and Srijaranai, S., *J. Photochem. Photobio., A: Chem.* **43,** 329 (1988).
43. Turchi, C. S., and Ollis, D. F., *J. Catal.* Submitted.